

# Combined effect of carbon surface area and sodium lignosulfonate interaction in lead-acid batteries: microstructural and electrochemical aspects

Rocha, G. K.<sup>1,\*</sup>, Skovroinski, E.<sup>2</sup>, Santos, A. J. V<sup>3</sup>., Souza, W. M.<sup>1</sup>, Lima Filho, M. R. F.<sup>4</sup> and Torres, S. M.<sup>1</sup>

<sup>1</sup>Universidade Federal da Paraíba - PPGEM, Joao Pessoa, Paraíba 58051-900 Brazil

<sup>2</sup>Instituto de Tecnologia Edson Mororó Moura, Belo Jardim, Pernambuco, Brazil

<sup>3</sup>Universidade Federal da Paraíba, Departamento de Engenharia Elétrica, João Pessoa, Paraíba 58051-900 Brazil

<sup>4</sup>Universidade Federal da Paraíba, Departamento de Engenharia de Materiais, Joao Pessoa, Paraíba 58051-900 Brazil

## Abstract

Energy storage is essential for advancing green energy solutions, with the lead-acid battery market expected to grow by 4.4 percent a year until 2029, reaching USD 58.65 billion. Lithium-ion batteries, although predominant, face challenges such as cost, stability, safety, and environmental impacts, including a lack of efficient recycling. On the other hand, lead-acid batteries, with a 99 percent recycling rate in the US, offer a more sustainable option. Hybrid Electric Vehicles (HEVs) play a crucial role in fuel economy and pollutant reduction, requiring batteries with good dynamic charge acceptance. Problems such as sulphation in lead batteries are mitigated with additives such as carbon and sodium lignosulphonate, which improve performance. This study focuses on optimizing the composition of battery pastes, maximizing charge acceptance by analyzing the interaction between carbon and sodium lignosulphonate, to improve the efficiency and competitiveness of lead-acid batteries by evaluating their electrochemical and electrical properties.

Keywords: Dynamic Charge Acceptance. Lead-acid battery. Energy storage. Carbon black. Specific Surface area.

## INTRODUCTION

Energy storage systems are strategic pivots when it comes to the success of implementing effective chains for so-called green or clean energies. The U.S. Department of Energy (DOE) predicts over 100 GWh of growth worldwide by 2030 for the Energy Storage (ESS) market. The lead-acid battery market is estimated to grow with a compound annual growth rate (CAGR) of 4.4% until 2029, reaching a market size of USD 58.65 billion, while for the lithium battery market, the rate could get 20%, reaching a market value of USD 200 billion as early as 2027 [1].


Accumulators are becoming increasingly important for modern vehicles and in solar and wind plant installations. For many years acting only as an auxiliary power source, used for starting, lighting, and ignition (SLI) of automotive vehicles. Understanding that the transport chain represents the second largest source of polluting gas emissions in the world, advances in accumulators now occupy an essential role in the traction system, both in Modern Hybrid Electric Vehicles (HEVs) or in the case of Fully Electric Vehicles (EVs), allowing them to act as a complete replacement for the internal combustion engine [2,3]. In these cases, the most used type of battery has been lithium-ion which,

when compared to other rechargeable batteries, such as Ni-Cd, Ni-MH, and also lead-acid, stands out for its high energy and power density, plus long service life. However, for this application, many batteries need to be grouped in series and parallel to form a battery pack and deliver the power necessary to drive the vehicle. This creates problems of cost, stability, consistency, and safety, thus limiting the applications of lithium-ion batteries [4].

In addition to these limitations, the lithium-ion battery presents a significant disadvantage from an environmental point of view, as there is no established process for recycling it. The extraction and processing of lithium can cause environmental damage, such as soil and water pollution, due to the use of toxic chemicals and the improper disposal of waste. In addition, the increased production of these materials can also result in the degradation of local ecosystems and the emission of greenhouse gases associated with extraction, processing, and transport activities [5].

Therefore, the depletion of lithium reserves and the corresponding price increase the desire for alternative types of batteries. In this scenario, the continuous study of the lead battery, especially associated with the use of hybrid electric vehicles, is necessary [6]. Besides its variation in cell shapes and sizes, lithium-ion batteries require a variety of resources in their cells such as lithium, cobalt, and graphite, which require specific technologies and regulations for a complete recycling system making the recyclability very challenging. On the other hand, lead-acid batteries rely primarily on lead

\* [grace.060.gk@gmail.com](mailto:grace.060.gk@gmail.com)

 <https://orcid.org/0009-0002-9581-4076>

and sulfuric acid, they have a well-established recycling system, with a 99% recycling rate in the USA, which contributes to a more sustainable life cycle. Recycling lead from batteries can reduce the demand for new sources of lead, thus mitigating the environmental impacts associated with its extraction and processing [7].

Hybrid electric vehicles (HEVs) have great potential to save fuel and reduce pollution emissions, so much research has focused on HEV technologies and applications in both academia and industry [8]. The use of HEV associated with the use of biofuel, for example, can represent an effective reduction in the negative impacts that the transport chain brings to the environment.

When using this type of vehicle, the importance of dynamic load acceptance (DCA) is highlighted. This property directly affects the efficiency and speed of battery recharging. The same occurs in the case of lead-acid batteries, especially in operating conditions at high current rates in partial state of charge (HRPSoC) [9]. These conditions are crucial for hybrid vehicles, as their batteries are often partially discharged and recharged with intense current pulses during braking [10].

Charge acceptance in batteries is strongly influenced by the surface quality of the active material on the negative electrode. HRPSoC operating conditions favor the appearance of large lead sulfate crystals, a phenomenon called plate sulfation. Larger crystals are more difficult to shrink during battery recharging, which leads to a progressive reduction in the battery capacity over its life [11]. To avoid the passivation of negative electrodes, it is common to use materials known as expanders, such as carbon, sodium lignosulfonate, and barium sulfate.

Carbon plays a crucial role due to its ability to store and conduct electrical charge. During battery discharge, carbon forms a conductive network around the lead sulfate crystals, providing an efficient route for electron flow [12]. Furthermore, high surface area carbons have a porous structure that allows the formation of an electrical double layer at the solid-liquid interface when immersed in the battery electrolyte. Because of this, high surface area carbons can store a significant amount of electrical charge [13]. Meanwhile, lignosulfonate acts as a film-forming agent on the electrode, creating a polyelectrolyte layer on the surface of the lead. This layer has the function of preventing the formation of the lead sulfate passivating layer, contributing to improving battery performance [14].

By exploring the dynamics of the interaction between carbon and sodium lignosulfonate it is possible to optimize the composition of the battery paste to maximize its dynamic charge acceptance capacity (DCA) and, consequently, improve its performance in real operating conditions, in addition, the optimization of contents can allow the cost reduction of batteries while maintaining their quality and performance, making them more competitive in the market.

In this work, a systematic investigation of the interaction between high and low surface area carbons with sodium lignosulfonate was carried out based on electrical tests

focusing on dynamic charge acceptance in lead battery cells.

## MATERIALS AND METHODS

Two carbons were selected, one with a low surface area ( $<50 \text{ m}^2/\text{g}$ ) and the other with a high surface area ( $>1400 \text{ m}^2/\text{g}$ ) based on the manufacturer's specification. The carbons will be called LSA (low surface area) and HSA (high surface area). This approach aims to highlight possible disparities in electrical results more clearly.

To produce the negative paste lead oxide, barium sulfate, sodium lignosulfonate, carbon black, synthetic fibers, and a sulfuric acid solution (with a concentration of  $1,4 \text{ g}\cdot\text{mL}^{-1}$ ) were mixed in a bench mixer, forming a consistent paste. The amounts of lead oxide, barium sulfate, fiber, and sulfuric acid remained constant, while the amounts of carbon and sodium lignosulfonate varied according to Table II.

To make the plates, lead grids were used, and to make the cells, separators made from polyethylene and a polypropylene box were used. In total 13 cells were produced for each carbon. Each cell was composed of two positive plates and one negative plate, with a theoretical capacity of 5Ah and a voltage of 2V.

The carbons were placed directly in the sample holder of the Bruker equipment, model D8 Advance, using a glass plate to acquire the diffractograms. The process lasted 1 hour, with increments of  $0.02^\circ$  and an acquisition time of 1 s for each step. The analysis was conducted using CuK $\alpha$  radiation.

The analyses were carried out using the Raman/AFM system, an OmegaScope from the Horiba brand. Composed of an iHR32 spectrometer, with a 671 nm excitation laser and a maximum power of 50 mW, coupled to the AIST-NT SmartSPM microscope and a spectral range of  $800\text{-}2000 \text{ cm}^{-1}$ .

The carbonic materials were analyzed using SHIMADZU equipment, model DTG-60H, with a heating ramp from  $25^\circ\text{C}$  to  $1000^\circ\text{C}$ , with a heating rate of  $10^\circ\text{C}\cdot\text{min}^{-1}$ .

In this investigation, the TESCAN, MIRA3 LMU equipment was used. Microscopic images were captured at magnifications of up to 30,000x using high-resolution scanning mode, with an accelerating voltage of 15 kV and an average working distance of 10 mm. In the process of prior preparation of the samples, gold metallization was carried out.

For this analysis, Micromeritics equipment, model Tristar II, was used, using nitrogen gas as adsorbate at a temperature of 77.35 K, and the results were modeled by the BET isotherm.

Table I - Definition of levels for experimental analysis

Controllable factors	Levels (%)	
	Minimum	Maximum
Carbon concentration (x)	0.5	1.5
Lignosulfonate concentration (y)	0.4	0.7

Table II - Experimental design for the production of prototypes

Sample	Run	Factor 1 - Carbon (%)	Factor 2 - Lignosulfonate (%)
1	11	0.5	0.2
2	1	1.5	0.2
3	10	0.5	0.7
4	8	1.5	0.7
5	4	0.29	0.45
6	6	1.71	0.45
7	7	1	0.1
8	3	1	0.8
9	13	1	0.45
10	5	1	0.45
11	2	1	0.45
12	9	1	0.45
13	12	1	0.45

The experimental design, statistical analyses, and surface of responses were conducted using the Design-Expert 13 Software developed by State-ease. The details of the tests and the limits of the variables can be seen in Table I:

The evaluated arrangement was composed of 2 factors of 2 levels ( $2^k = 2^2 = 4$ ), four axial points ( $2k = 4$ ), and 5 central points, totaling 13 combinations. The experiments were performed randomly to avoid bias. The software generated a sequence of experiments, presented in Table II that were performed on the 2V prototypes, and their numerical results were computed.

Statistical parameters were estimated using ANOVA, with a confidence level of 95%. For the models obtained, LSA and HSA carbons were designated as A and sodium lignosulfonate as B.

For this work, four discharge cycles were conducted by the protocols stipulated by the ABNT NBR 15940 standard [15]. In the first cycle, the nominal capacity was determined as 5Ah, calculated based on the active material present in the cell. Subsequent capacities were adjusted to reflect actual capacity after each subsequent cycle. The initial current ( $I_{20}$ ) was established at 0.25A, with a voltage cut-off limit set at 1.75V, considering that the cells evaluated were 2V each.

To ensure comparability of capacity results, the relationship between cell capacity and active material weight was calculated. This allowed us to obtain the specific capacity, expressed in Ah/g.

The test was carried out by EN 50342-6:2015 [16]. This standard establishes three stages for the test: the first is battery conditioning, also known as pre-cycling; the second is the qDCA test (quick DCA), which evaluates the battery's charge acceptance capacity after the charge ( $I_c$ ) and discharge ( $I_d$ ) cycles; Finally, there is the DCRss test, which analyzes the behavior of battery charge acceptance in a start-stop ( $I_r$ ) simulation.

The tests carried out in this work only covered the conditioning and quick DCA stages, as these are the stages that exert the greatest influence on the total result ( $I_{DCA}$ ).

The test carried out for the prototypes in this study was an adaptation of the ABNT NBR 15940:2013 standard, being carried out at room temperature (25°C) applying a constant overvoltage of 2.667V measured for a period of 500h. The battery is weighed before and after the test, and the result is given by the relationship between the difference in weight, initial and final, and the capacity ( $C_{20}$ ) of the battery.

## RESULTS AND DISCUSSIONS

Initially, an evaluation of the internal structure of the materials was carried out, using specific surface area (SBET) and particle size measurements, which were obtained through  $N_2$  adsorption and scanning electron microscopy, respectively.

The LSA carbon presented a surface area of 22.21  $m^2 g^{-1}$ , with a particle size of 200 nm while the HSA presented an  $S_{BET}$  of 1,355.04  $m^2 g^{-1}$  and a particle size of 20 nm. It can be seen from the results that the surface area of carbon increases as the particle diameter decreases.

Scanning electron microscopy analysis revealed that both LSA and HSA particles have a spherical shape, with a regular particle size distribution, around 20 nm for HSA and around 200 nm for LSA. Furthermore, an increase in the formation of carbon agglomeration was observed as particle size decreased. This agglomeration influences the rheological and dispersion properties of carbons in the paste [17]. Figure 1 presents the micrographs obtained from the carbon samples analyzed.

The materials were also analyzed for X-ray diffraction (XRD). The diffractograms obtained are illustrated in Figure 2.

Both carbons do not present a characteristic diffraction peak, just a halo in the  $2\theta$  region between approximately 20 and 27°, which characterizes them as amorphous materials. This also can be observed when compared with the graphite diffractogram, which presents a well-defined and intense crystallographic peak around 26.4°, referring to the (002) plane. This peak is characteristic of the distance between the graphene layers, which is approximately 0.34 nm in this structure. Furthermore, another peak characteristic of graphite, although with lower intensity, occurs around 54.4°, referring to the (004) plane [18]. A broad peak at 101 was observed, particularly evident on HSA carbon. These results confirm that carbon blacks are amorphous carbons [19].

About Raman analysis, this technique makes it possible to estimate the relative concentration of amorphous carbon on the surface of carbon black aggregates. The average size of nanocrystallites can be determined through variations in the position, width, and intensity of two distinct Raman peaks, observed at 1345  $cm^{-1}$  (peak D, associated with the disorder) and 1575  $cm^{-1}$  (peak G, associated with graphite). The shape of these peaks is influenced by the size of the crystallites [20].

When observing the RAMAN spectra obtained for LSA

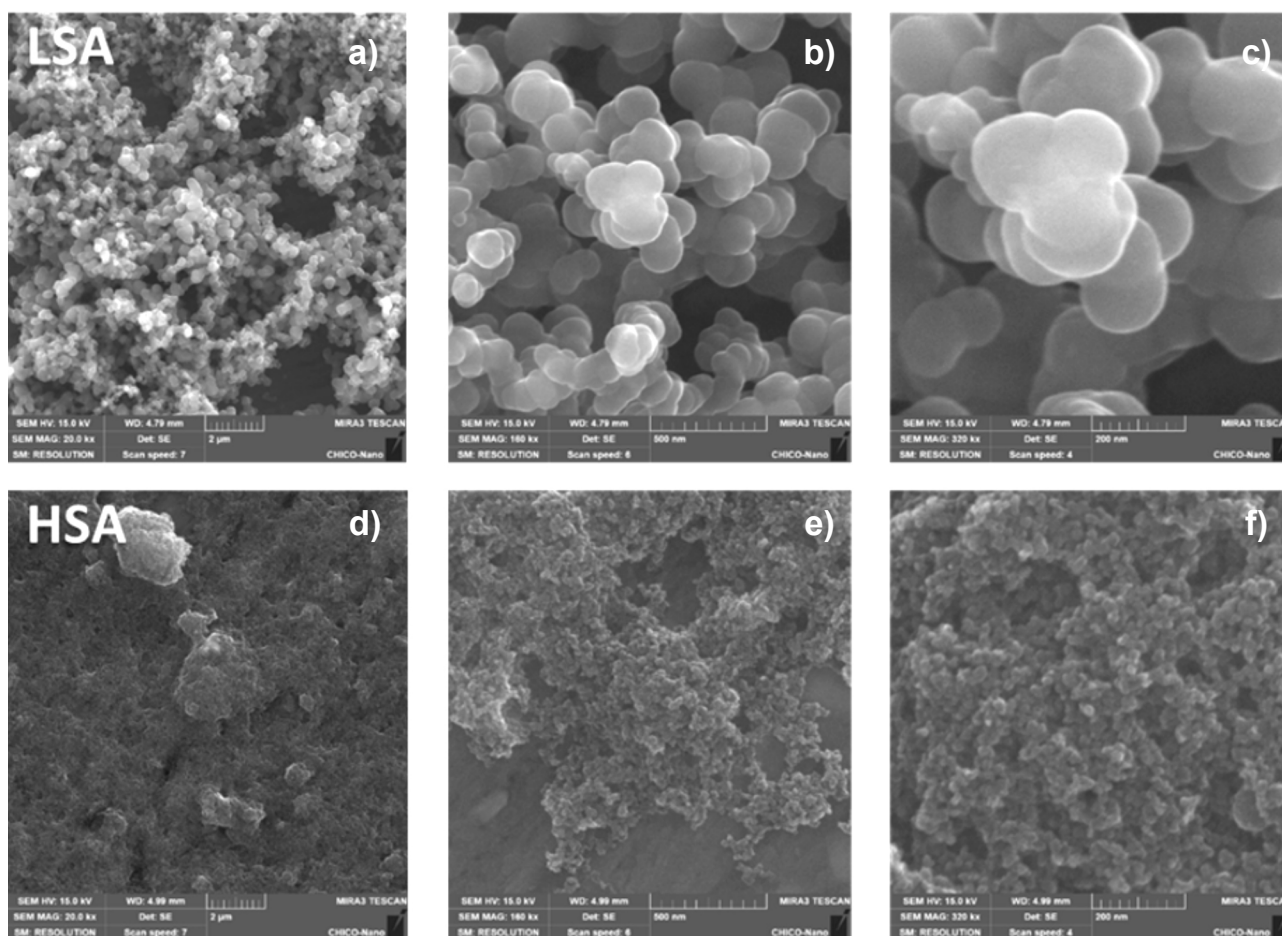


Figure 1: Comparison between microscopies of LSA and HSA samples.

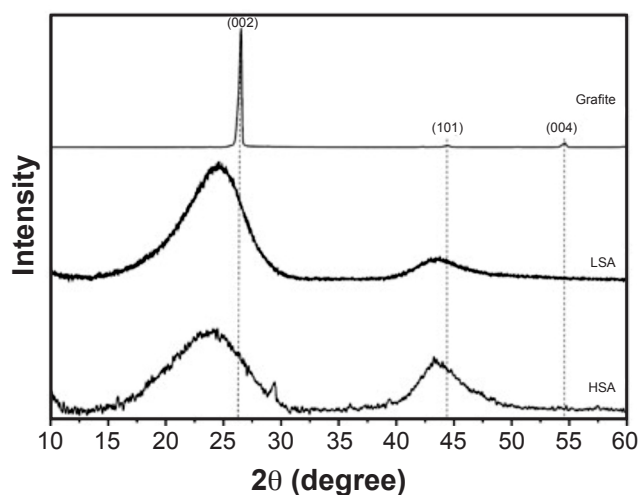


Figure 2: X-ray diffraction diagrams for LSA and HSA carbons.

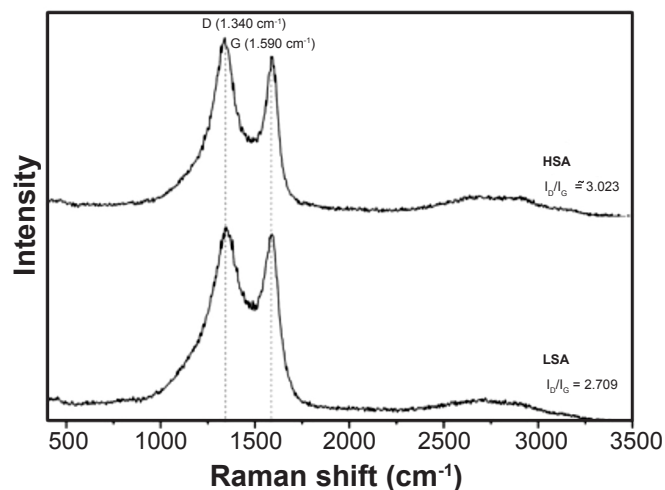


Figure 3: RAMAN spectra for LSA and HSA carbons.

and HSA carbons, Figure 3, the presence of many defects in both structures stands out, as evidenced by the high intensity of the D bands.  $I_D/I_G$  values greater than 1 indicate the presence of a significant amount of defects in the structure. On the other hand,  $I_D/I_G$  values lower than 1 indicate materials with fewer structural defects and, consequently, a

more cohesive graphitic network [21, 22]. When compared, HSA carbon exhibits a higher ID/IG ratio, corroborating that its structure is more amorphous.

The samples were subjected to thermogravimetric (TG) analysis, the results of which are presented in Figure 4.

Thermogravimetric (TG) analysis provides information



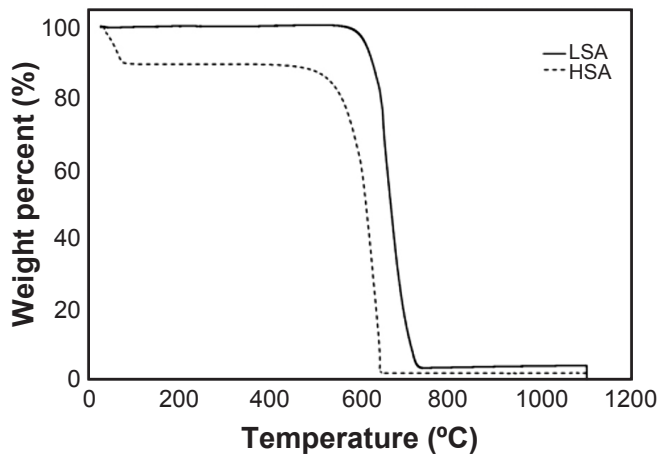


Figure 4: Thermogravimetric curves obtained from LSA and HSA carbons.

about its thermal stability, decomposition, and the presence of impurities in carbon blacks.

From Figure 4 it can be seen that LSA is classified as the most thermally stable compound when compared to HSA, since the degradation of HSA mass occurs at a lower temperature (518°C) than LSA (600°C). This occurs because a greater surface area allows greater exposure to oxygen, favoring the combustion reaction [23].

From the TG curves obtained for LSA and HSA, the presence of 3 main mass loss events is verified, as shown in Table III.

Between 35°C and 100°C, the first event occurs for HSA carbon, characterized by a mass loss of 10%. This event can be attributed to the evaporation of water and volatile compounds present in the carbon structure. Due to its high surface area, HSA tends to absorb these materials.

The second event observed between 490°C and 650°C, is the result of oxidation of the HSA carbon structure. Analysis of the thermograms reveals that HSA has its carbon structure completely oxidized at around 650°C. LSA carbon goes through this oxidation process between 570°C and 740°C. The two carbons showed less than 5% residual mass at the end of the analysis. Table IV presents a summary of the characterization of the two carbons, LSA and HAS.

The analysis of the results obtained in this phase highlights the significant influence of the surface area in determining the characteristics of the material. It was observed that an increase in surface area is associated with a smaller particle diameter with more particle agglomeration. The intensity of the D band in the Raman spectrum also demonstrated a positive correlation with the surface area. X-ray diffraction results confirmed that carbon blacks have an amorphous structure. Furthermore, during the thermogravimetric (TG) analysis, it was observed that materials with a larger surface area tend to show earlier degradation at lower temperatures, highlighting the influence of the surface area on the thermal stability of the material. These observations show the critical importance of surface area in determining material properties and behavior, it is a fundamental parameter to be considered in future studies and applications.

Table V presents a summary of the statistical analysis for the specific capacity analysis, considering the two carbons, LSA and HSA.

In this analysis, the two models obtained were considered statistically significant. Being a quadratic model for LSA carbon and a linear for HSA carbon.

A diagnostic analysis of the data was carried out to check whether there were any outliers or leverage effects in the responses. The normality graph, Figure 5, indicates that there are no outliers or unusual observations, making data adjustment unnecessary.

After statistical analysis of the models, they were plotted. Figure 6 illustrates the contour and surface graphs for the two models obtained.

From the analysis, it is observed that the variation in the concentration of lignosulfonate and LSA carbon about the specific capacity follows a quadratic pattern, being influenced by both the carbon concentration and the lignosulfonate concentration. On the other hand, the variation in lignosulfonate and HSA carbon concentrations follows a linear pattern, with the lignosulfonate concentration exerting a greater influence on the specific capacity results. Higher values of this response are observed in regions with high lignosulfonate concentration and low carbon concentration.

However, when analyzing the magnitude of the results

Table III - Mass loss events of LSA and HSA samples from thermogravimetric (TG) analysis.

Carbon	Weight loss (%)			Residual mass
	35 °C – 100 °C	490 °C – 650 °C	570°C – 740 °C	
LSA	-	-	97%	3%
HSA	10%	88%	%	2%

Table IV - Summary of LSA and HSA carbon characterization results.

	$S_{BET}$ ( $m^2g^{-1}$ )	$D_{part}$ (nm)	$I_D/I_G$	Degradation temperature (°C)
LSA	22.21	200	2.71	570°C – 740 °C
HSA	1,355.04	20	3.02	490 °C – 650 °C

Table V - ANOVA results for specific capacity.

	LSA	HSA
Model type	Quadratic	Linear
Significant terms	A; A <sup>2</sup> ; B <sup>2</sup>	B
Mean	0.145	0.142
R <sup>2</sup>	0.885	0.547
Adeq precision	11.89	6.9

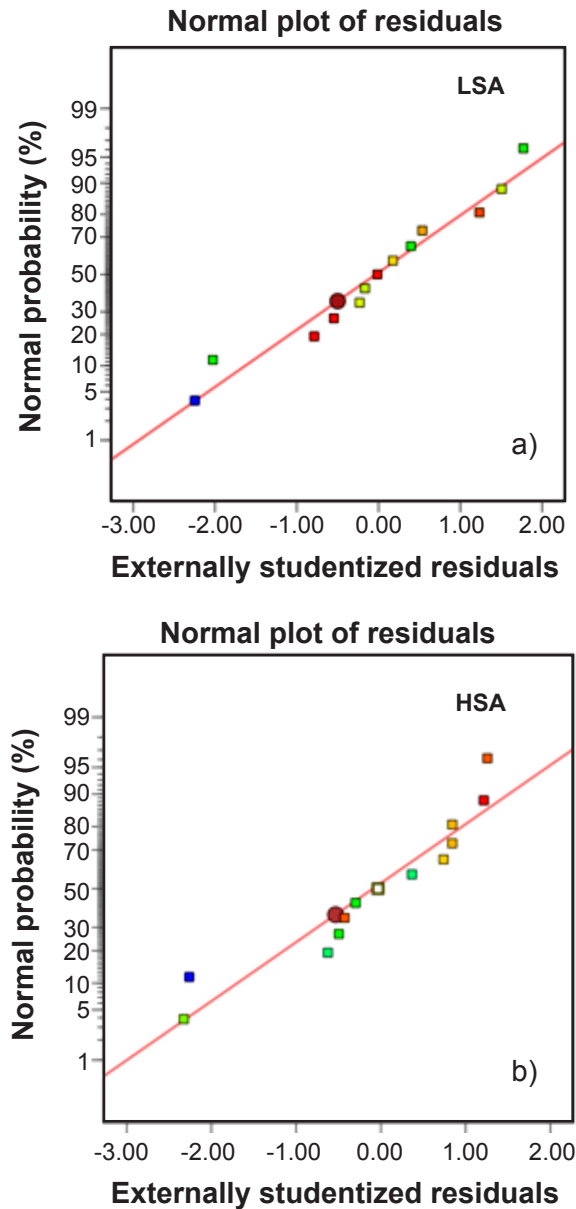


Figure 5: Normal probability percentage chart for specific capacity.

through their means and standard deviations, Figure 7, it is observed that there is no statistically significant difference between the samples with the two types of carbon. This suggests that the specific capacity is not impacted by the use of high or low surface area carbon in the negative active

material. This result is in line with the findings of Kumar *et al.* (2018) in their study [14].

The charge acceptance analysis was carried out in two stages. The first stage considers all responses in adjusting the model, and the second stage disregards the most discrepant responses in the group, thus obtaining a more adjusted model.

For the first analysis, table VI presents a summary of the statistical analysis for the dynamic charge acceptance analysis, considering the two carbons, LSA and HSA.

The proposed quadratic and linear models fit the system. The coefficient of determination (R<sup>2</sup>) indicated a more accurate model fit for the LSA carbon system than for the HSA. This result is confirmed by the accuracy adequacy indicator.

Additionally, a diagnostic analysis of the data was conducted to identify possible outliers or leverage effects on responses. Figure 8 illustrates the residual normality graph used for this analysis.

When carrying out the dispersion analysis of the results, it was observed that for the two carbons evaluated, the combination of 1% Carbon (LSA or HSA) + 0.1% Sodium Lignosulfonate represents an outlier.

However, considering the context of the study, the point in question represents a particular case. The use of 0.1% sodium lignosulfonate in combination with a high concentration of carbon (1%) configures an extreme situation, where a maximum load acceptance is observed, Figure 9.

In previous studies, an inverse effect caused by sodium lignosulfonate on DCA results was identified. It was found that DCA decreases as the concentration of sodium lignosulfonate in the formulation increases. This behaviour can be attributed to the effect of carbon coating by lignosulfonate, which impairs the participation of certain carbon regions in the negative plate charging and discharging process, according to the model illustrated in Figure 10 [17].

The result obtained reinforces the observation that the presence of lignosulfonate reduces the conductivity/capacitance of carbon, resulting in lower charge acceptance. An interesting aspect of this result is the significant difference in the other responses, even when compared to the results obtained with 0.2% lignosulfonate. This suggests that there may be a minimum concentration of lignosulfonate required to influence the outcome of DCA.

A new analysis was performed, removing outliers from

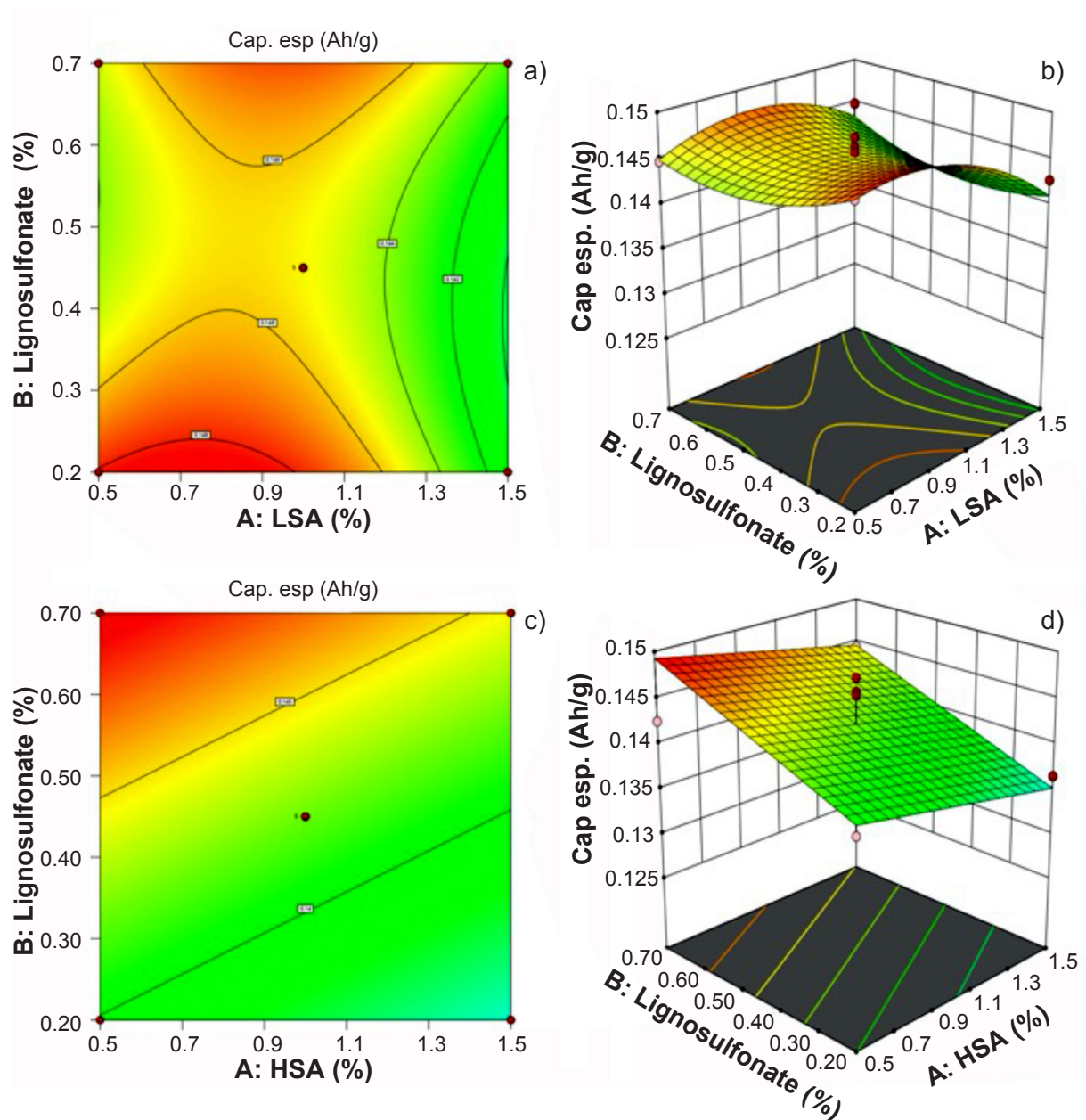


Figure 6: Contour and surface plots for specific capacity about variation in concentration of lignosulfonate and LSA and HSA carbon.

the models. The contour and surface graphs obtained are illustrated in Figure 11.

From the models obtained, it is possible to observe that the surface area of the carbon exerts a significant influence on the load acceptance result. The average DCA result for LSA carbon was 0.19 A/Ah while for HSA carbon, 0.45 A/Ah, representing an increase of 137% when a carbon with a larger surface area was applied. Furthermore, in the LSA/Lignosulfonate system, the curvature of the response indicates that there is a significant interaction between carbon and lignosulfonate in this system, with the lignosulfonate concentration exerting the greatest influence on the DCA result. On the other hand, in the HSA/Lignosulfonate system, the linear result suggests that there is no significant interaction between the two materials. Therefore, carbon

with a larger surface area has a greater influence on the DCA result than the lignosulfonate concentration or low surface area carbon. Figure 9 depicts a possible mechanism of carbon/lignosulfonate interaction, the more carbon area available, the higher the DCA. The surface area of HSA and LSA carbons are very different, 1,355.04 and 22.21  $\text{m}^2 \text{g}^{-1}$ , respectively, when the lignosulfonate interacts with the carbon, an important portion of the LSA may be covered by the lignosulfonate, whereas for HSA carbon the coverage is quite negligible, considering the same amount of lignosulfonate on the paste formulation and this may be the reason for absence of lignosulfonate influence on DCA when HAS was used.

As in previous analyses, water consumption was evaluated using ANOVA, and diagnostic graphs were

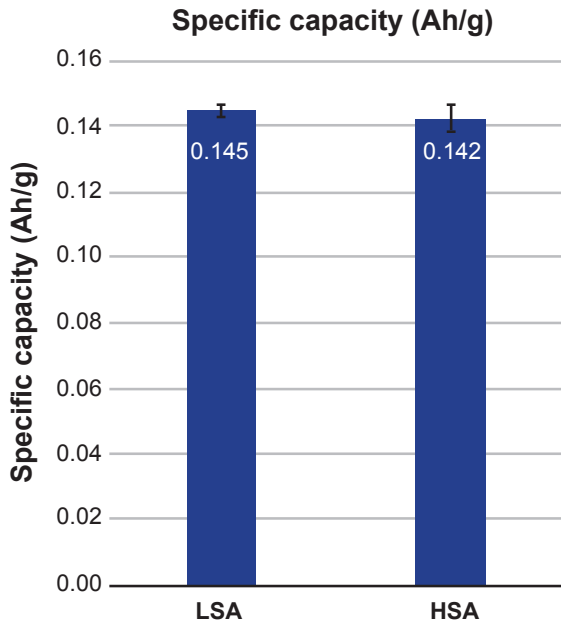


Figure 7: Comparison between the average specific capacity results for LSA and HSA carbons.

examined to verify the normality of the results. After identification, outliers were removed from the analysis. The identified outliers did not represent specific cases and, therefore, the statistical analysis presented in Table VII and the contour and surface plots illustrated in Figure 12 present the results after removing the outliers from the analysis.

After the necessary adjustments, both models were considered statistically significant. Both presented a coefficient of determination greater than 0.8, indicating that a high proportion of data variability is explained by statistical models.

In both cases, it was observed that there was an interaction between the lignosulfonate and the applied carbon. It was also observed that lignosulfonate had a mitigating effect on water consumption, while the surface area of carbon had a negative effect, considerably increasing the battery's water consumption. This was evidenced by the average 192.2% increase in water consumption when HSA carbon was applied compared to LSA carbon.

The results obtained in this research highlight the importance of carbon surface area for dynamic charge

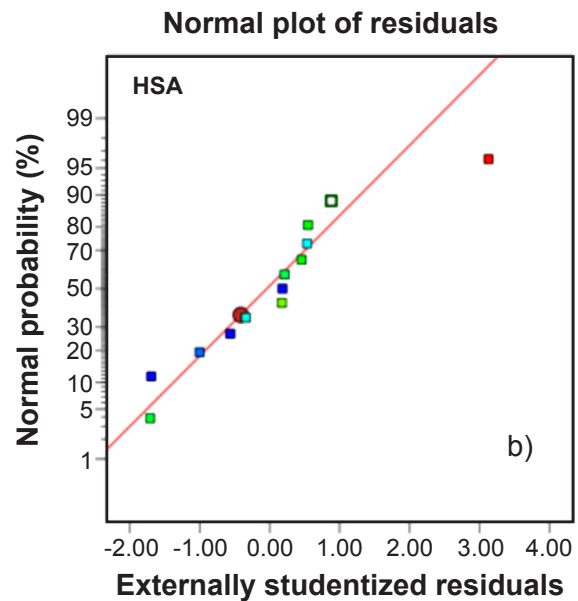
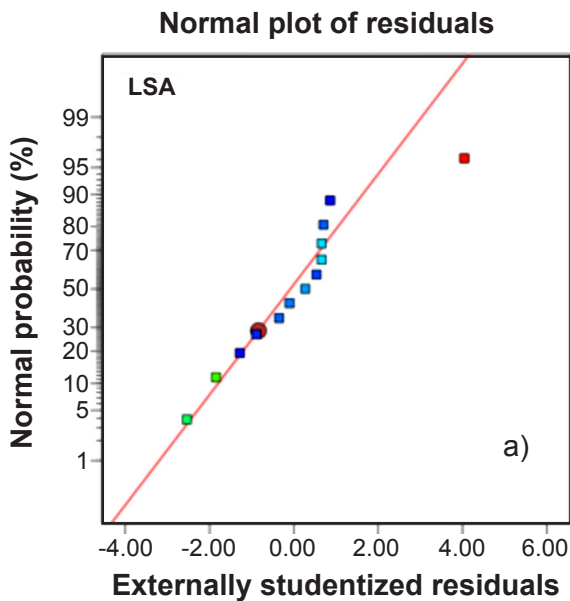


Figure 8: Normal percentage probability graph for DCA.

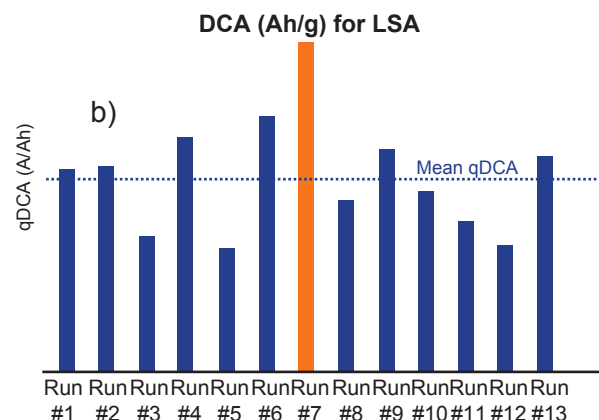
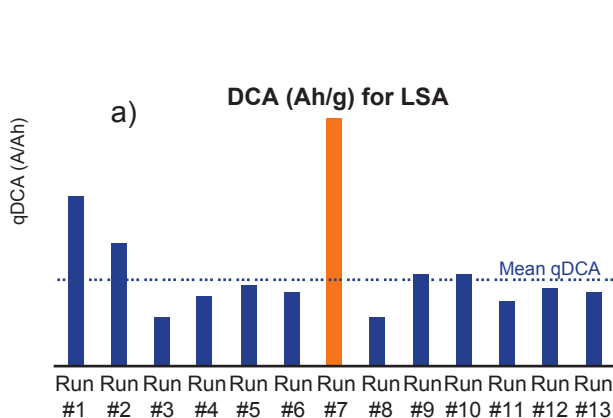


Figure 9: Numerical results for DCA of LSA and HSA carbons.



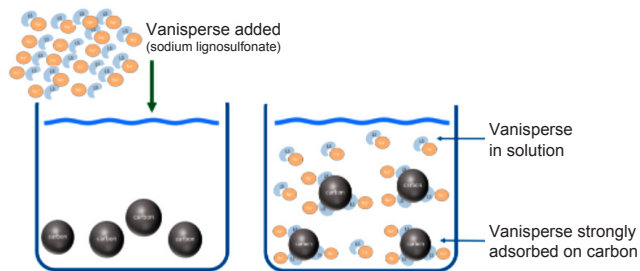


Figure 10: Mechanism of adsorption of sodium lignosulfonate to carbon [17].

Table VI - ANOVA results for DCA.

	LSA	HSA
Model type	Quadratic	Linear
Significant terms	B, B <sup>2</sup>	-
Mean	0.22	0.48
R <sup>2</sup>	0.936	0.465
Adeq precision	14.79	6.13

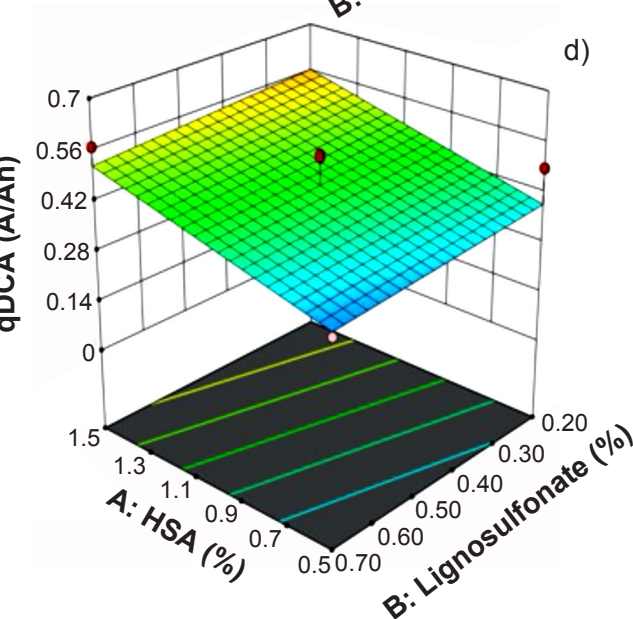
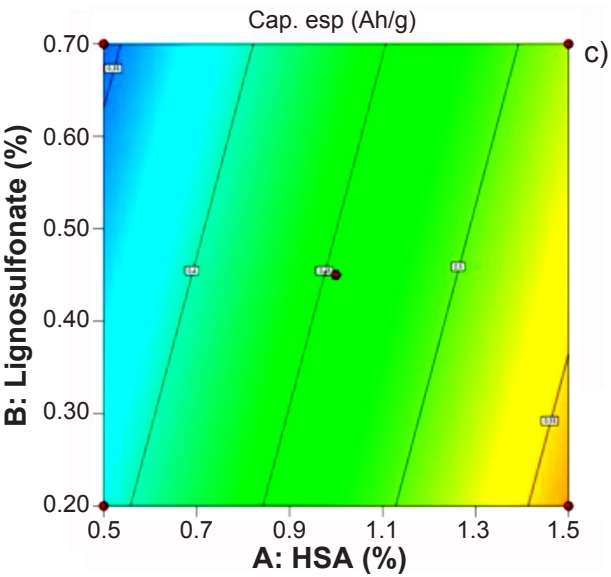
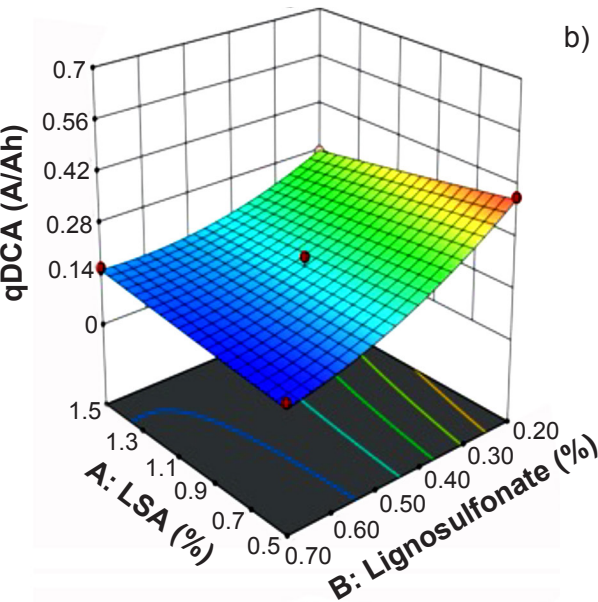
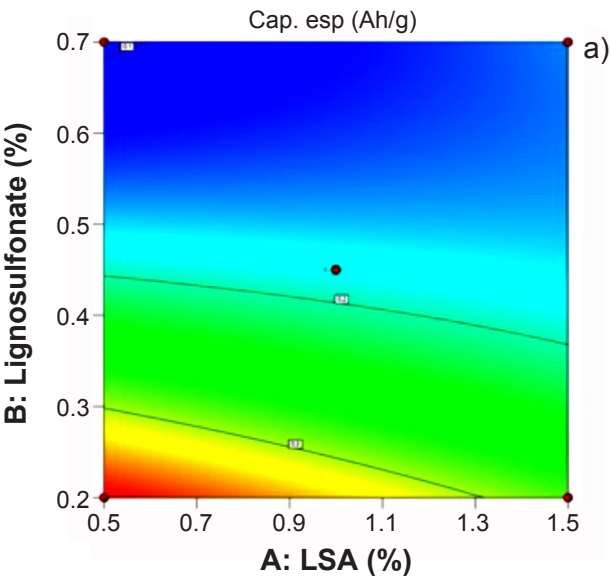


Figure 11: Contour and surface plots for DCA about variation in carbon lignosulfonate concentration (LSA and HSA) without influence of the outlier.

acceptance. The analyses carried out showed that the surface area exerts a significant influence on the properties of the carbonaceous materials evaluated, affecting both their

structural characteristics and their electrical performance. From the systems analysis, it was observed the strong influence that the interaction between carbon and lignosulfonate

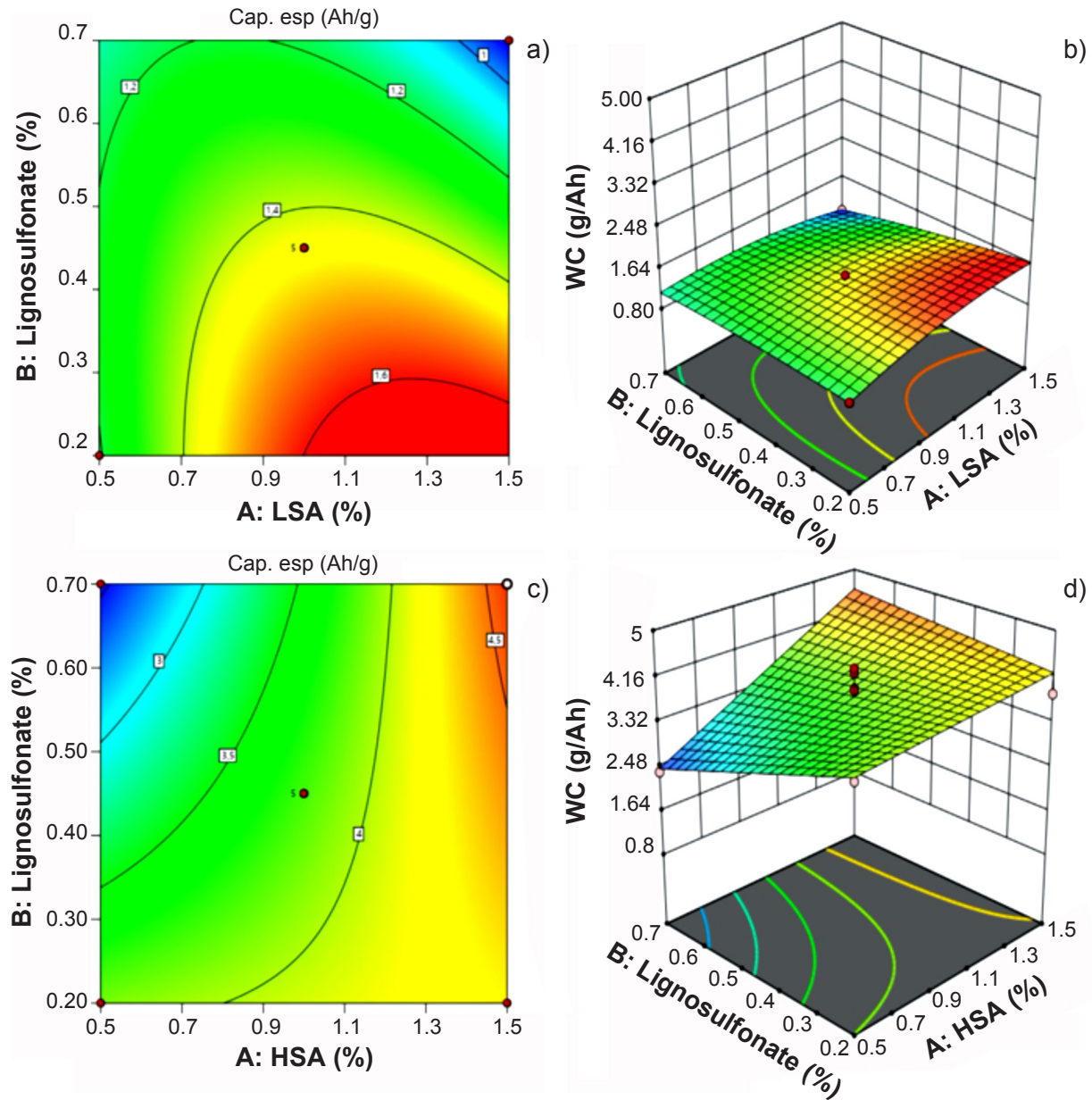


Figure 12: Contour and surface graphs for water consumption about variation in lignosulfonate and carbon concentration (LSA and HSA).

Table VII - ANOVA table for water consumption.

	LSA	HSA
Model type	Quadratic	2FI
Significant terms	A; B; AB	A; AB
Mean	1.29	3.77
R <sup>2</sup>	0.997	0.827
Adeq precision	64.05	11.46

has on the acceptance of dynamic load. Furthermore, the application of the response surface methodology has proven to be effective for quickly and accurately conducting analyses, providing results efficiently and reliably.

These findings provide valuable insights for the development and optimization of materials for application

in lead-acid batteries.

This work demonstrated that the lignosulfonate and carbon content added to the negative plate has a strong influence on DCA and water consumption of lead-acid cells. On the other hand, the type of carbon used has a very strong influence on the results, both in DCA and water consumption. For the industry, these results are important for several reasons: (i) Optimization of contents can allow cost reduction without reducing battery quality; (ii) The design of a battery is always designed considering the final application of the product, thus, with the help of the results presented, it is possible to design a product that meets the demand for which it is planned, optimizing the paste formulation and costs.

These aspects can improve competitiveness by

optimizing products and reducing costs.

## CONCLUSIONS

From the characterizations carried out with the carbons, it was possible to identify the significant influence exerted by the surface area on the characteristics of the materials evaluated. It was observed that the increase in surface area is directly related to the smaller particle diameter of carbonaceous materials. Analysis of X-ray and Raman diffractograms indicated that carbon with a higher surface area has a more amorphous structure compared to carbon with a low surface area. The results of the thermogravimetric analysis suggested that the surface area influences the thermal stability of the material, indicating that materials with a higher surface area may be less thermally stable compared to materials with a lower surface area.

Regarding the electrical tests, in the analysis of the specific capacity it was noted that the surface area of the carbon did not have a significant influence on the result nor did the amount of sodium lignosulfonate.

The dynamic charge acceptance analysis revealed an inverse effect caused by lignosulfonate on the results of this variable. A maximum DCA point was identified for both systems when the concentration of lignosulfonate in the formulation was minimal. In the LSA/Lignosulfonate system, the observed curvature indicates that there is an interaction between these two components. On the other hand, in the HSA/Lignosulfonate system, no interaction was observed between the two components. In this case, the carbon concentration is decisive for the DCA results. When compared, it was observed the significant influence of the surface area on DCA, with the average result of the system with HSA carbon being 137% greater than that of the system with LSA carbon.

From the analysis of water consumption, it was observed that the surface area increases the result of this variable, however, the lignosulfonate concentration mitigated water consumption. When comparing the averages of the two systems, an increase of 192.2% was observed with the use of HSA carbon about LSA carbon.

These results highlight the importance of carbon surface area and the interaction between carbon and sodium lignosulfonate as fundamental elements for dynamic load acceptance. They also emphasize the need to employ optimization techniques to maximize these results, as increasing this variable may be associated with side effects such as increased water consumption in the battery.

## REFERENCES

[1] Mordor Intelligence. Lead Acid Battery Market Size & Share Analysis - Growth Trends & Forecasts (2024 - 2029). 23 de fevereiro de 2024. Disponível em: <https://www.mordorintelligence.com/industry-reports/lead-acid-battery-market>. doi:10.1016/b978-0-323-96022-9.00327-3.

[2] Chen Q, Lai X, Huang G, Tian X, Gao F, Han X, Zheng Y. Investigating carbon footprint and carbon reduction potential using a cradle-to-cradle LCA approach on lithium-ion batteries for electric vehicles in China. *J Clean Prod.* 2022;**369**:133342. doi:10.1016/j.jclepro.2022.133342.

[3] Smith MJ. Improvements in testing and performance of batteries for automotive applications [dissertação]. The University of Sheffield, South Yorkshire, England; 2018. doi:10.4324/9780429045905-3.

[4] Chen W, Liang J, Yang Z, Li G. A review of lithium-ion battery for electric vehicle applications and beyond. *Energy Procedia.* 2019;**158**:4363-68. doi:10.1016/j.egypro.2019.01.783.

[5] Costa CM, Barbosa JC, Gonçalves R, Castro H, Campo FJ. Recycling and environmental issues of lithium-ion batteries: Advances, challenges and opportunities. *Energy Storage Mater.* 2021;**37**:433-65. doi:10.1016/j.ensm.2021.02.032.

[6] Biemoolt J, Jungbacker P, Teijlingen T, Yan N, Rothenberg G. Beyond lithium-based batteries. *Materials.* 2020;**13**:425. doi:10.3390/ma13020425.

[7] Huang B, Peng Z, Song X, An L. Recycling of lithium-ion batteries: Recent advances and perspectives. *J Power Sources.* 2018;**399**:274-86. doi:10.1016/j.jpowsour.2018.07.116.

[8] Li L, You S, Wang X, Yang C. Structure optimization and generalized dynamics control of hybrid electric vehicles. *Modeling, Dynamics and Control of Electrified Vehicles.* 2018;207-44. doi:10.1016/B978-0-12-812786-5.00006-9.

[9] Bozkaya B, Settelein J, Giffin GA, Bauknecht S, Kowal J, Karden E. Lithium-ion battery chemistries for high-power applications. *Energy Technol.* 2022;**10**(2):2101051. doi:10.1002/ente.202101051.

[10] Lam LT, Louey R. Development of ultra-battery for hybrid-electric vehicle applications. *J Power Sources.* 2006;**158**:1140-48. doi:10.1016/j.jpowsour.2006.03.022.

[11] Lach J, Wróbel K, Wróbel J, Podśadni P, Czerswiński A. Applications of carbon in lead-acid batteries: A review. *J. Solid State Electrochem.* 2019;**23**:693-705. doi:10.1007/s10008-018-04174-5.

[12] Zimáková J, Fryda D, Vaculík S, Baca P, Bouska M. Examination of impact of lignosulfonates added to the negative active mass of a lead-acid battery electrode. *J. Energy Storage.* 2018;**18**:229-38. doi:10.1016/j.est.2018.04.009.

[13] Meiws HB, Schulte D, Kowal J, Sauer DU, Heck R, Karden E. Dynamic charge acceptance of lead-acid batteries: Comparison of methods for conditioning and testing. *J Power Sources.* 2012;**207**:30-36. doi:10.1016/j.jpowsour.2011.12.045.

[14] Kumar S, Babu N, Kumar SK, Prasad S, Balaji G, Jagadish M. Influence of carbon and interaction of carbon and lignosulfonate on dynamic charge acceptance of flooded lead acid batteries. *Int J Sci Res.* 2018;**7**:1940-46.

[15] Associação Brasileira de Normas Técnicas (ABNT). ABNT NBR 15940:2013: Baterias chumbo-ácido para uso em veículos rodoviários automotores de quatro ou mais rodas – Especificação e métodos de ensaio. *Manuais*

de Normalização para Trabalhos Acadêmicos. 2013. doi:10.21728/p2p.2024v10n2e-6919.

[16] European Committee for Standardization (CEN). EN 50342-6:2015: Lead-acid starter batteries - Batteries for Micro-Cycle Applications. 2015. doi:10.3403/30363337u.

[17] McNally T, Abney C, Shafarik S. Assessment of carbon black - expander interactions on capacity, dynamic charge acceptance, cold cranking and partial state of charge life in lead batteries. *ELBC*. 2022.

[18] Anakli D, Aksoy C. Synthesis of graphene oxide through ultrasonic assisted electrochemical exfoliation. *Open Chem*. 2019;**17**:581-86. doi:10.1515/chem-2019-0062.

[19] Lee S, Lee SH, Roh JS. Analysis of activation process of carbon black based on structural parameters obtained by XRD analysis. *Crystals*. 2021;**11**:153. doi:10.3390/cryst11020153.

[20] Ungar T, Gubicza J, Ribárik G, Pantea C. Microstructure of carbon blacks determined by X-ray diffraction profile

analysis. *Carbon*. 2002;**40**:929-37. doi:10.1016/S0008-6223(01)00224-X.

[21] Oliveira AEF, Pereira AC, Bettio GB, Tarley CRT. Síntese, estudo e caracterização estrutural da redução térmica e com hidrazina do óxido de grafeno por espectroscopia Raman e espectroscopia de infravermelho. *Rev Virtual Quím*. 2019;**11**(3):866-77. doi:10.21577/1984-6835.20190060.

[22] Matos CFD. Materiais nanocompósitos multifuncionais formados por látices poliméricos e grafeno ou óxido de grafeno: síntese, caracterização e propriedades [tese de doutorado]. Universidade Federal do Paraná; 2015. doi:10.47749/t/unicamp.2019.1094081.

[23] Netzsch. Carbon Black. Acessado em 31 de janeiro de 2024. Disponível em: <https://analyzing-testing.netzsch.com/en/training-know-how/glossary/carbon-black>.

(Rec. 25-Feb-2024, Rev. 21-Jun-2024, Ac. 24-Sep-2024)

(AE: F. M. B. Marques)

